

Infrared dielectric function of GaAs_{1-x}P_x semiconductor alloys near the reststrahlen bands

Cite as: Appl. Phys. Lett. **123**, 172102 (2023); doi: [10.1063/5.0173978](https://doi.org/10.1063/5.0173978)

Submitted: 26 August 2023 · Accepted: 11 October 2023 ·

Published Online: 23 October 2023



View Online



Export Citation



CrossMark

Stefan Zollner,^{1,a)}  Shivashankar R. Vangala,²  Vladimir L. Tassev,²  Duane Brinegar,^{2,3} and Samuel Linser^{2,3} 

AFFILIATIONS

¹Department of Physics, New Mexico State University, MSC 3D, P.O. Box 30001, Las Cruces, New Mexico 88003-8001, USA

²Air Force Research Laboratory (AFRL), Sensors Directorate, Wright-Patterson AFB, Ohio 45433, USA

³KBR, Inc., Beavercreek, Ohio 45431, USA

^{a)} Author to whom correspondence should be addressed: zollner@nmsu.edu. URL: <http://femto.nmsu.edu>

ABSTRACT

The infrared dielectric function of thick GaAs_{1-x}P_x alloy layers grown on (001) GaAs substrates by hydride vapor phase epitaxy was investigated in the reststrahlen region using Fourier-transform infrared ellipsometry. The spectra are influenced by the Berreman artifact at the longitudinal optical phonon frequency of the GaAs substrate and by interference fringes due to the finite layer thickness. The ellipsometric angles were analyzed to determine the dielectric function of the alloy layer. Two-mode behavior, including strong GaAs-like and GaP-like optical phonons, was observed, confirming the results of Verleur and Barker [Phys. Rev. **149**, 715 (1966)]. Due to the increased sensitivity of ellipsometry in the reststrahlen region, several weak phonon features could also be seen. The lattice absorption peaks are asymmetric and show side bands at the lower and higher frequencies. A single additional peak, as suggested by the percolation model, does not describe the spectra. The cluster model proposed by Verleur and Barker is a better fit to the data. Due to the broadening of the phonon absorption peaks, the authors were unable to find a unique decomposition into multiple components.

Published under an exclusive license by AIP Publishing. <https://doi.org/10.1063/5.0173978>

The long-wavelength optical phonons of compound semiconductor alloys have long been an active area of research. While the infrared (IR) lattice response of binary zinc blende compounds, such as GaAs¹⁻⁴ and GaP,⁴⁻⁶ can be described quite well with a simple Lorentzian resulting in one reststrahlen band between the transverse optical (TO) and longitudinal optical (LO) phonon energies, at least two such reststrahlen bands are found in many semiconductor alloys. Genzel, Martin, and Perry⁷ explained that the long-wavelength phonons of mixed crystals can be represented by four classes, which they called one-mode, two-mode, and intermediate. The early experimental evidence was reviewed by Chang and Mitra.⁸

GaAs_{1-x}P_x alloys display two-mode behavior:^{7,8} Since the reststrahlen bands of GaAs and GaP are separated by a large energy gap (73 cm⁻¹), two distinct GaAs-like and GaP-like phonon bands appear in the alloy over the complete range of compositions. These bands shift with composition, but they never overlap. As pointed out by Humlíček,⁹ IR reflection (including ellipsometry) measurements are very sensitive to weak absorption processes within the reststrahlen band. Therefore, several smaller IR absorption peaks were also detected

in GaAs_{1-x}P_x alloys^{10,11} but could not be explained with two-phonon absorption. Weak secondary peaks were also found in Raman scattering experiments.^{12,13} Different explanations were given for these weak peaks, especially the cluster model^{10,14} and the percolation model.¹⁵

While theoretical interest in the nature of these weak peaks has continued,^{14,15} calculations are still compared to 50 year-old IR reflectance data.¹⁰ Therefore, a reexamination of the IR lattice response of GaAs_{1-x}P_x alloys using modern IR ellipsometry equipment is overdue. That is the purpose of this manuscript. Our measurements of thick relaxed epitaxial layers grown on GaAs lead to a minor inconvenience, the Berreman artifact at the LO mode of the substrate and interference fringes due to the finite thickness, but this can be resolved with optical modeling of the thin-film response. As far as we know, alloy phonons have only been studied previously with IR ellipsometry for wurtzite semiconductor nitride alloys^{16,17} and for various metal oxides with low crystal symmetry,¹⁸ but not for zinc blende semiconductor alloys.

GaAs_{1-x}P_x alloys have been used historically for red light emitting diodes.¹⁹ More recent interest has been for compact, high-power, tunable laser sources for middle to long wavelength IR (3–14 μm)

operation, which are in great demand for a wide variety of applications.^{20,21} These include critical military applications, such as proactive and post launch IR countermeasures, enhanced laser radar for ranging, target recognition, and 3D holography, and reliable long-range IR communication, as well as applications in security such as remote sensing and spectroscopy of chemicals and biological species, medical applications like breath analysis, and science applications like ultrafast spectroscopy of chemical reaction dynamics. However, since the available direct coherent sources in this spectral range do not satisfy requirements for power, tunability, and frequency coverage associated with such applications, frequency conversion through phase or quasi-phase matching in nonlinear optical materials was suggested as a reasonable alternative for developing such sources for this important frequency range. GaAs_{1-x}P_x as a combination of two of the most studied to date quasi-phase matching materials, GaAs and GaP, is especially attractive by the possibility to engineer a material with lower two-photon absorption than GaAs but higher nonlinear susceptibility than GaP, a material that could be, eventually, pumped with the readily available sources from the telecommunication waveband. The use of GaAs_{1-x}P_x alloys for multijunction solar cells has also been discussed.²²

Thick GaAs_{1-x}P_x alloy layers with compositions ranging from $x = 0.20$ to 0.80 were grown by low-pressure hydride vapor phase epitaxy (HVPE) on (001) oriented GaAs substrates as described elsewhere.²¹⁻²⁴ This growth method is very fast and some variations in composition should be expected. This becomes apparent in x -ray diffraction (XRD) and ellipsometry measurements near the direct bandgap. The alloy composition was determined using high-resolution XRD and room-temperature photoluminescence.²⁵ A linear variation of the lattice constant with composition (Vegard's Law) was assumed.¹⁰ We described the variation of the direct bandgap of GaAs_{1-x}P_x alloys with the bowing parameter of $b = -0.19$ eV recommended in Ref. 26, within the range of parameters determined by electroreflectance.^{27,28} A list of samples is given in Table S1. A few samples only produced diffuse reflections from a red alignment laser but, nevertheless, had good IR ellipsometry spectra.

The ellipsometric angles²⁹ ψ and Δ of several thick GaAs_{1-x}P_x alloy layers on GaAs were acquired at room temperature from 250 to 8000 cm⁻¹ using a J. A. Woollam Fourier-transform IR variable angle of incidence spectroscopic ellipsometer (FTIR-VASE) as described in the supplementary material. Since ellipsometry measures two parameters (an amplitude $\tan \psi$ and a phase Δ) at each wavelength and angle of incidence, it is usually possible to extract the real and imaginary parts of the dielectric function of the layer without a Kramers-Kronig transformation, if the complex dielectric function of the substrate and the layer thickness are known. One can also build models for the complex dielectric functions of the substrate and layer that depend on parameters as described below. A good introduction to spectroscopic ellipsometry is given in the textbook by Fujiwara and Collins.²⁹

The phonon parameters for the GaAs and GaP binary endpoints were determined with measurements on reference substrates as described in Ref. 6 by fitting with a simple Lorentzian

$$\epsilon(\omega) = \epsilon_{\infty} + \frac{A\Omega_{\text{TO}}^2}{\Omega_{\text{TO}}^2 - \omega^2 - i\Gamma_{\text{TO}}\omega}. \quad (1)$$

We did not find it necessary to include different broadening parameters for the transverse (TO) and longitudinal optical (LO) phonons due to anharmonic decay. The Lorentzian, then, has three parameters,

the amplitude A , the TO phonon energy Ω_{TO} , and the broadening parameter Γ_{TO} . The energy of the corresponding LO phonon can be estimated from the Lyddane-Sachs-Teller relation⁶

$$\Omega_{\text{LO}}^2 = \Omega_{\text{TO}}^2 \left(\frac{A}{\epsilon_{\infty}} + 1 \right). \quad (2)$$

Equation (2) assumes frequency-independent screening of the Fröhlich interaction by the high-frequency dielectric constant ϵ_{∞} . This approximation is probably accurate for the GaP-like phonon with the higher energy. The GaAs-like phonon might be screened a little more, since the dielectric constant between the GaAs-like and GaP-like phonons is larger than ϵ_{∞} . Therefore, we might slightly overestimate the LO phonon energy of the GaAs-like mode when using Eq. (2).

The ellipsometry data for a typical sample (225B) with a phosphorus content of 61.5%, within the percolation regime,¹⁵ are shown in Fig. 1 in the reststrahlen region from 250 to 500 cm⁻¹ in several representations, as ellipsometric angles ψ and Δ , pseudodielectric function $\langle \epsilon \rangle$, and pseudodissipation function $-1/\langle \epsilon \rangle$. A detailed interpretation of the raw data are given in the supplementary material.

The spectrum was fitted with a sum of two Lorentzian oscillators to describe the GaAs-like and GaP-like phonons, shown by dotted lines in Fig. 1. Parameters obtained from the fit are given in Table S1. The corresponding LO energies were estimated from the Lyddane-Sachs-Teller relation (2). Solid vertical lines in Fig. 1 show the TO energies obtained from this fit. There is qualitative agreement, especially for the pseudodielectric function, but the agreement could be better. As expected, two Lorentzians are not sufficient to describe the complex vibrational spectra of the GaAs_{1-x}P_x alloy.

The fit to the GaP-like band with a single Lorentzian (dotted) is particularly poor. As discussed by Humlíček,^{9,30} the impact of a weak absorption feature is amplified, if it occurs within a reststrahlen band. The shape of this GaP-like reststrahlen band allows the conclusion that the main GaP-like TO/LO phonon pair has energies of about 355 and 400 cm⁻¹, with a second weaker absorption peak located within these boundaries.

In summary, the main features of the raw ellipsometry data in Fig. 1 for sample 225B can be interpreted if the GaAs-like and GaP-like reststrahlen bands and the Berreman artifact^{31,32} at the TO energy of the GaAs substrate are taken into account. There are also small modifications due to the finite thickness of the alloy (interference effects).

Since a fit to the data with two Lorentzians to describe the GaAs-like and GaP-like vibrations was only partially successful, we added a second (weaker) GaP-like TO phonon, as suggested by the percolation theory of Pagès *et al.*,¹⁵ at an energy of about 12 cm⁻¹ above the stronger one. This reduced the mean standard deviation (weighted by errors), also called MSE, by about 20%, but still did not provide a good description of ψ in the GaP-like reststrahlen region.

The agreement between the model and the data for sample 225B can be improved further if a total of eight Lorentzian oscillators are introduced to describe the lattice absorption. Results are shown by the solid lines in Fig. 1. Even such a large number of oscillators does not achieve a perfect fit to the data. It is questionable whether such a large number of Lorentzian parameters carries physical significance. We believe that our FTIR ellipsometry data do not contain enough information to perform meaningful fits with 6 to 10 Lorentzian for comparison with energies and amplitudes predicted by the cluster model theory, which was carried out in Ref. 14.

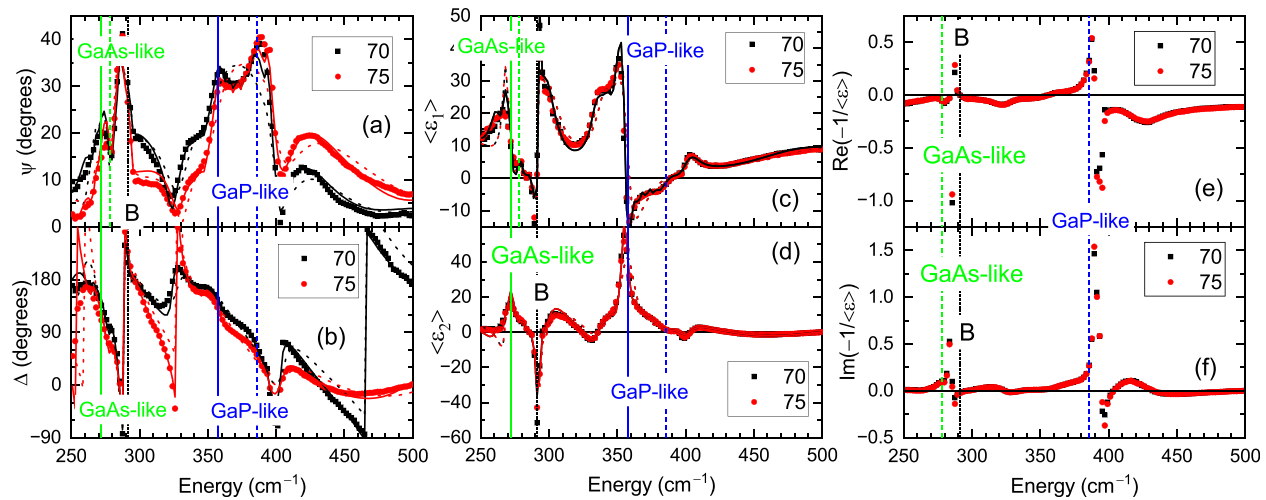


FIG. 1. Ellipsometric angles ψ (a) and Δ (b), real (c), and imaginary (d) parts of the pseudodielectric function and of the pseudolos function [(e) and (f)] for sample 225B with 61.5% P. The symbols show experimental data at two angles of incidence. The dotted vertical line labelled “B” indicates the Berreman artifact at the LO energy of the GaAs substrate. The green and blue lines show the energies of the TO (solid) and LO (dashed) phonons of the GaAs-like and GaP-like phonons of the alloy. Fits to the data with two and eight Lorentzians are given by dotted and solid lines, respectively.

The ellipsometric angles ψ for six selected alloys and the binary endpoints are shown in Fig. 2 (symbols) together with the best fit with a single Lorentzian for the GaAs-like and GaP-like optical phonons (lines). As expected, the areas under the reststrahlen bands and the TO/LO splittings scale with composition. The Berreman artifact and some interference effects are also seen.

Since a Lorentzian fit describes the data only qualitatively, we also fitted the ellipsometric angles with a Kramers–Kronig-consistent B-spline

function²⁹ to approximate the dielectric function. The results are shown in Figs. S1 and 3. The TO peak heights and areas scale with composition, but the GaAs-like and GaP-like TO peaks are clearly separated for all compositions, as expected for two-mode behavior. The TO peaks are asymmetric and sometimes show weak sidebands. This could be in support of the cluster model¹⁰ or because of compositional variations in these HVPE-grown alloys.

The thickness, roughness parameters, high-frequency dielectric constant, TO and LO energies, and TO amplitudes and broadenings of

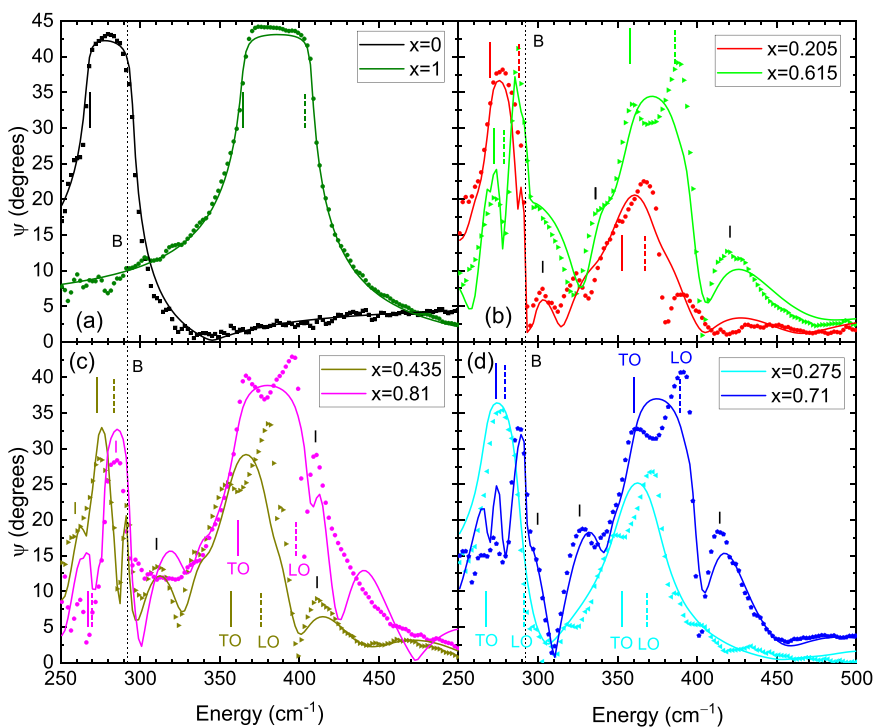


FIG. 2. The reststrahlen bands expressed by the ellipsometric angle ψ (symbols) measured at an incidence angle of 70° for bulk GaAs and GaP (a) and for thick GaAs_{1-x}P_x alloys on GaAs [(b)–(d)]. Solid lines show the best fit with a single Lorentzian for the GaAs-like and GaP-like optical phonons. The vertical dotted line shows the energy of the LO phonon in the GaAs substrate at 292 cm^{-1} , which causes a Berreman artifact for some samples. The short solid and dashed vertical lines mark the energies of the TO and LO modes, respectively. Peaks labelled “I” are interference fringes.

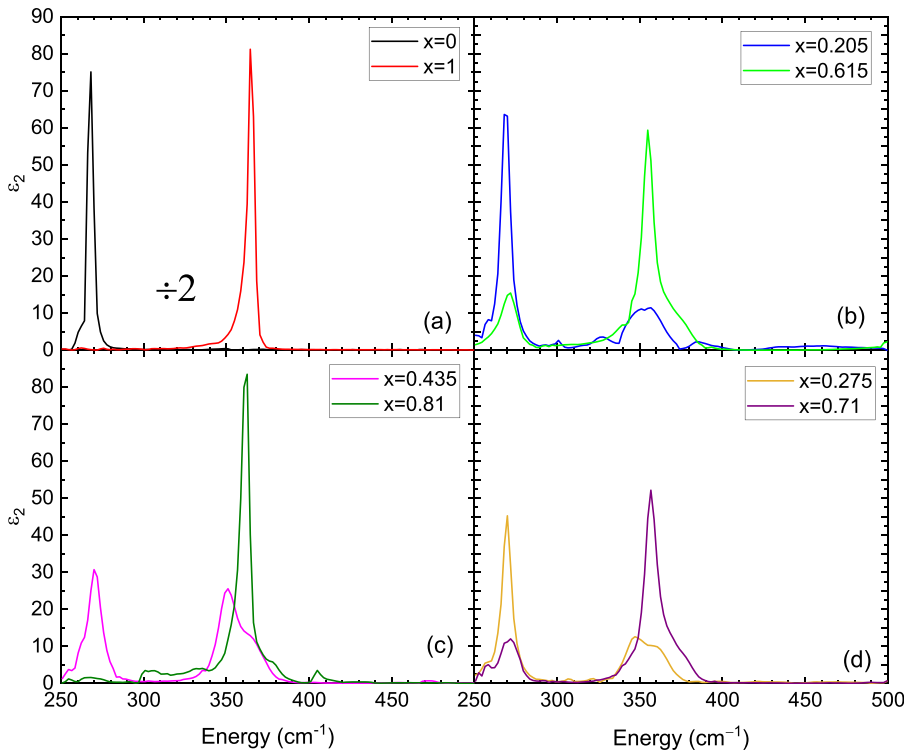


FIG. 3. Imaginary part of the dielectric function ϵ_2 for bulk GaAs and GaP (a) and for thick GaAs_{1-x}P_x alloys on GaAs [(b)–(d)] determined from a B-spline fit to the ellipsometric angles. The spectra were divided by two for the bulk substrates in (a) to fit on the same scale as the alloys. The corresponding figure for the real part is shown in the supplementary material. Compare with Fig. 2 in Ref. 14.

GaAs-like and GaP-like phonon modes for ten different compositions are given in Table S1. Energies, amplitudes, and broadenings are shown in Fig. 4. For most samples, the LO energies agree very well with the Raman shifts from Pistol and Liu,¹³ which confirms our use of the LST relation (2). The TO energies, which are not given in Ref. 13, were fitted with a linear relationship

$$\Omega_{\text{TO}}^{\text{GaP-like}} = 351.4(8) + 12.6(1.5)x \text{ meV}, \quad (3)$$

$$\Omega_{\text{TO}}^{\text{GaAs-like}} = 269.5 \pm 1.3 \text{ meV}. \quad (4)$$

The GaAs-like TO mode did not vary with composition within the errors of our data. The amplitudes of the TO modes scale approximately linearly with composition, as shown by the solid lines in Fig. 4(b). The broadenings of the GaAs-like TO mode are small (about 5 cm⁻¹) across the entire range of compositions.

On the other hand, the broadenings of the GaP-like mode are large for small P contents and then decrease linearly with increasing x . This was also found by Verleur and Barker¹⁰ and is strong evidence in support of the cluster model.¹⁴

We also determined the dielectric function and the complex refractive index of our GaAs_{1-x}P_x alloy layers in the vicinity of the direct bandgap E_0 and the dependence of E_0 on composition^{33–35} (see the supplementary material).

In summary, the infrared ellipsometry spectra of thick GaAs_{1-x}P_x alloy layers grown on GaAs (001) by HVPE show strong GaAs-like and GaP-like reststrahlen bands due to optical phonon lattice absorption. The amplitudes and TO/LO phonon splittings vary with composition as expected. A model for the infrared dielectric

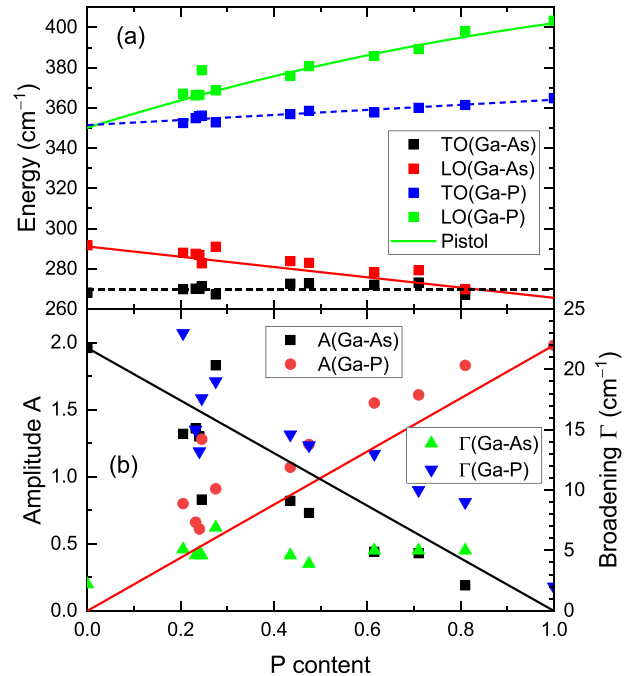


FIG. 4. (a) Energies of TO and LO phonons from FTIR ellipsometry (symbols) in comparison with the LO energies from Ref. 13 (solid) and a linear fit to the TO energies (dashed) and (b) amplitudes and broadenings of TO phonons. Straight lines scale the amplitudes with composition.

function based on a single Lorentzian for each mode describes the ellipsometry data only qualitatively due to weak side bands, which are particularly pronounced for the GaP-like mode for low P contents. This is strong evidence in support of the Verleur and Barker cluster model.^{10,14} There is insufficient information in our spectra to deconvolute our peaks into six to ten Lorentzians. A single additional GaP-like mode shifted by 12 meV, as suggested by the percolation model,¹⁵ does not describe our data. Results for the optical constants near the direct bandgap are also presented.

See the supplementary material for additional details about samples and methods, a detailed interpretation of the raw data for one sample, and visible ellipsometry results near the direct bandgap.

This research was supported in part by the Air Force Research Laboratory Sensors Directorate, through the Air Force Office of Scientific Research Summer Faculty Fellowship Program (Contract Nos. FA8750-15-3-6003, FA9550-15-0001, and FA9550-20-F-0005). V.L.T. and S.R.V. acknowledge the support from the Air Force Office of Scientific Research (Program Manager Dr. John Luginsland) under Award No. FA9550-22RYCOR003. We are grateful to Dr. T. E. Tiwald for guiding us through the use of B-spline functions for fitting IR ellipsometry data.

AUTHOR DECLARATIONS

Conflict of Interest

The authors have no conflicts to disclose.

Author Contributions

Stefan Zollner: Formal analysis (lead); Funding acquisition (equal); Investigation (lead); Visualization (lead); Writing – original draft (lead); Writing – review & editing (lead). **Shivashankar Vangala:** Conceptualization (lead); Funding acquisition (lead); Investigation (equal); Writing – review & editing (supporting). **Vladimir L. Tassev:** Funding acquisition (equal); Investigation (equal); Writing – original draft (supporting). **Duane Brinegar:** Investigation (supporting). **Samuel Linser:** Investigation (supporting).

DATA AVAILABILITY

The data that support the findings of this study are available from the corresponding author upon reasonable request.

REFERENCES

- ¹A. H. Kachare, W. G. Spitzer, F. K. Euler, and A. Kahan, *J. Appl. Phys.* **45**, 2938 (1974).
- ²R. T. Holm, J. W. Gibson, and E. D. Palik, *J. Appl. Phys.* **48**, 212 (1977).

- ³E. D. Palik, in *Handbook of Optical Constants of Solids*, edited by E. D. Palik (Academic, New York, 1998), p. 429.
- ⁴D. J. Lockwood, G. Yu, and N. L. Rowell, *Solid State Commun.* **136**, 404 (2005).
- ⁵A. S. Barker, *Phys. Rev.* **165**, 917 (1968).
- ⁶N. S. Samarasingha and S. Zollner, *J. Vac. Sci. Technol. B* **39**, 052201 (2021).
- ⁷L. Genzel, T. P. Martin, and C. H. Perry, *Phys. Status Solidi B* **62**, 83 (1974).
- ⁸I. F. Chang and S. S. Mitra, *Adv. Phys.* **20**, 359 (1971).
- ⁹J. Humlíček, *Thin Solid Films* **313–314**, 687 (1998).
- ¹⁰H. W. Verleur and A. S. Barker, *Phys. Rev.* **149**, 715 (1966).
- ¹¹Y. S. Chen, W. Shockley, and G. L. Pearson, *Phys. Rev.* **151**, 648 (1966).
- ¹²N. D. Strahm and A. L. McWorter, in *Proceedings of the Conference on Light Scattering Spectra in Solids*, edited by G. B. Wright (Springer, New York, 1969), p. 455.
- ¹³M. E. Pistol and X. Liu, *Phys. Rev. B* **45**, 4312 (1992).
- ¹⁴J. Cebulski, M. Woźny, and E. M. Sheregii, *Phys. Status Solidi B* **250**, 1614 (2013).
- ¹⁵O. Pagès, J. Souhaby, A. V. Postnikov, and A. Chafi, *Phys. Rev. B* **80**, 035204 (2009).
- ¹⁶R. Schmidt-Grund, M. Schubert, B. Rheinländer, D. Fritsch, H. Schmidt, E. M. Kaidashev, M. Lorenz, C. M. Herzinger, and M. Grundmann, *Thin Solid Films* **455–456**, 500 (2004).
- ¹⁷S. Schöche, T. Hofmann, D. Nilsson, A. Kakanakova-Georgieva, E. Janzén, P. Kühne, K. Lorenz, M. Schubert, and V. Darakchieva, *J. Appl. Phys.* **121**, 205701 (2017).
- ¹⁸M. Stokoy, T. Gramer, R. Korlack, S. Knight, S. Richter, R. Jinno, Y. Cho, H. G. Xing, D. Jena, M. Hilfiker, V. Darakchieva, and M. Schubert, *Appl. Phys. Lett.* **120**, 112202 (2022).
- ¹⁹M. G. Craford, R. W. Shaw, A. H. Herzog, and W. O. Groves, *J. Appl. Phys.* **43**, 4075 (1972).
- ²⁰V. Petrov, *Prog. Quantum Electron.* **42**, 1 (2015).
- ²¹L. Wang, S. R. Vangala, S. Popien, M. Beutler, V. L. Tassev, and V. Petrov, *Phys. Status Solidi (RRL)* **16**, 2200198 (2022).
- ²²A. Strömberg, G. Omanakuttan, Y. Liu, T. Mu, Z. Xu, S. Lourduodoss, and Y.-T. Sun, *J. Cryst. Growth* **540**, 125623 (2020).
- ²³V. L. Tassev and S. R. Vangala, *Crystals* **9**, 393 (2019).
- ²⁴V. Tassev, S. Vangala, D. Brinegar, M. Parker, and T. Barlow, *Phys. Status Solidi A* **218**, 2000443 (2021).
- ²⁵V. Petrov, L. Wang, S. Vangala, and V. Tassev, *Proc. SPIE* **11985**, 1198506 (2022).
- ²⁶I. Vurgaftman, J. R. Meyer, and L. R. Ram-Mohan, *J. Appl. Phys.* **89**, 5815 (2001).
- ²⁷A. G. Thompson, M. Cardona, K. L. Shaklee, and J. C. Woolley, *Phys. Rev.* **146**, 601 (1966).
- ²⁸D. E. Aspnes, *Phys. Rev. B* **14**, 5331 (1976).
- ²⁹H. Fujiwara and R. W. Collins, *Spectroscopic Ellipsometry for Photovoltaics* (Springer, Cham, 2018), Vol. 1.
- ³⁰T. I. Willett-Gies, C. M. Nelson, L. S. Abdallah, and S. Zollner, *J. Vac. Sci. Technol. A* **33**, 061202 (2015).
- ³¹D. W. Berreman, *Phys. Rev.* **130**, 2193 (1963).
- ³²J. Humlíček, *Phys. Status Solidi B* **215**, 155 (1999).
- ³³S. Zollner, J. Kircher, M. Cardona, and S. Gopalan, *Solid-State Electron.* **32**, 1585 (1989).
- ³⁴S. Zollner, M. Garriga, J. Kircher, J. Humlíček, M. Cardona, and G. Neuhold, *Phys. Rev. B* **48**, 7915 (1993).
- ³⁵S. Zollner, P. P. Paradis, F. Abadizaman, and N. S. Samarasingha, *J. Vac. Sci. Technol. B* **37**, 012904 (2019).

Supplementary Material for "Infrared Dielectric Function of GaAs_{1-x}P_x Semiconductor Alloys Near the Reststrahlen Bands"

(Dated: 26 August 2023)

Stefan Zollner,¹ Shivashankar R. Vangala,² Vladimir L. Tassev,² Duane Brinegar,^{2,3} and Samuel Linser^{2,3}

¹*Department of Physics, New Mexico State University, MSC 3D, P.O. Box 30001, Las Cruces, NM 88003, USA*

²*Air Force Research Laboratory (AFRL), Sensors Directorate, Wright-Patterson AFB, OH 45433, USA*

³*KBR, Inc., Beavercreek, OH, 45431, USA*

S1. DETAILS OF EXPERIMENTAL AND DATA ANALYSIS METHODS

The ellipsometric angles ψ and Δ and the depolarization spectra of several thick GaAs_{1-x}P_x alloy layers deposited on GaAs were acquired at room temperature from 250 to 8000 cm⁻¹ using a J. A. Woollam Fourier-transform IR variable angle of incidence spectroscopic ellipsometer (FTIR-VASE). Sample parameters are shown in Table SI. We selected 70° and 75° as the angles of incidence for our measurements, both below and above the mid-IR Brewster angles of the samples. We chose a resolution of 4 cm⁻¹. A smaller resolution increases the data acquisition time and the noise, while a larger resolution broadens the features of the spectra. Our choice of 4 cm⁻¹ seemed a good compromise for these samples. A smaller resolution is required for bulk GaP crystals, especially at low temperatures,⁶ but alloy disorder and small variations in composition increase our broadenings to values above 4 cm⁻¹. Measurements were performed with 15 compensator positions per revolution. To increase the signal-to-noise ratio, we averaged 200 interferometer mirror scans at each compensator position. Systematic errors were reduced with two $P=\pm 45^\circ$ polarizer positions and also zone-averaging the analyzer ($A=0^\circ, 90^\circ$). A typical measurement took about 18 hours per sample. WVASE32 and CompleteEase (J. A. Woollam Co., Lincoln, NE) ellipsometry software was used to analyze our data.

For each sample, we first restricted the analysis range to 500 to 8000 cm⁻¹. In this range, the ellipsometric angle Δ is close to 0° or 180° and the imaginary part of the pseudodielectric function $\langle\epsilon_2\rangle$ is very small (below 0.5), see Fig. S2. These data were used to fit the thickness of the surface layer, which we described using the Bruggeman effective medium approximation (BEMA) as a mixture consisting of 50% alloy layer and 50% voids. Typical surface layer thicknesses were between 20 and 50 Å, see Table SI. Next, we fitted the real part of the pseudodielectric function $\langle\epsilon_1\rangle$ to determine the alloy layer thickness (5 to 30 μm), the high-frequency dielectric constant ϵ_∞ , and the thickness nonuniformity (5 to 20%).

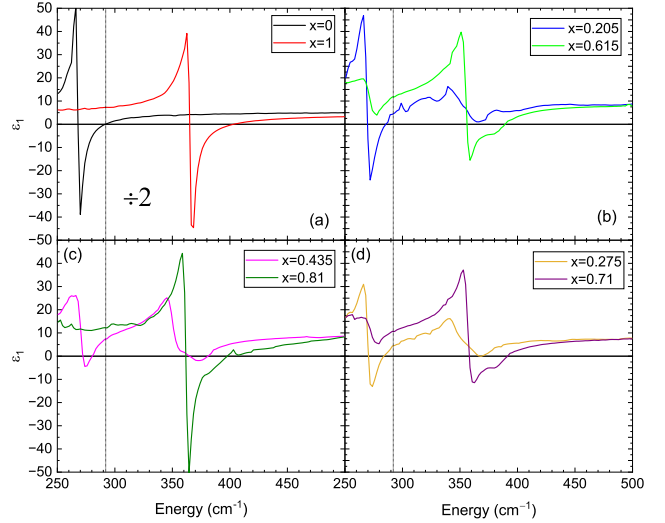


FIG. S1. Real part of the dielectric function ϵ_1 for bulk GaAs and GaP (a) and for thick GaAs_{1-x}P_x alloys on GaAs (b,c,d) determined from a B-spline fit to the ellipsometric angles. The spectra were divided by two for the bulk substrates in (a) to fit on the same scale as the alloys. The vertical lines show the LO mode of the GaAs substrate. The corresponding imaginary parts are shown in Fig. 3 in the main text.

These values were then fixed during the subsequent analysis of the phonon reststrahlen bands between 250 and 500 cm⁻¹, but iterative adjustments were sometimes required to achieve acceptable agreement between data and model over the complete spectral range. Since the layers were rather thick and nonuniform, the error was about 0.1 for ϵ_∞ and about 5-10% for the layer thickness. Perfect agreement between model and data above 500 cm⁻¹ could not be found due to thickness nonuniformity, which is difficult to model. The digital filter (convolution profile) used to describe thickness nonuniformity sometimes caused ringing as a function of photon energy. This was not important for the analysis of the phonon spectra at lower energies.

S2. DETAILED RESULTS FOR SAMPLE 225B WITH 61.5% PHOSPHORUS

The ellipsometry data for a typical sample (225B) with a phosphorus content of 61.5%, within the percolation regime,¹⁵ are shown in Fig. 1 in the reststrahlen region from 250 to 500 cm⁻¹ in several representations, as ellipsometric angles ψ and Δ , pseudodielectric function $\langle\epsilon\rangle$, and pseudoloss function $-1/\langle\epsilon\rangle$. The depolarization for this sample showed two strong peaks at 286 and 395

TABLE SI. Parameters of $\text{GaAs}_{1-x}\text{P}_x$ alloys and fit results, including P content x , As content $1 - x$, layer thickness t , surface layer thickness r , and high-frequency dielectric constant ϵ_∞ . The amplitudes A , energies Ω_{TO} , and broadenings Γ_{TO} of the GaAs-like and GaP-like transverse optical (TO) phonons are also given. 90% confidence limits are indicated in parentheses. The last two columns list the direct band gap E_0 and the refractive index n at $2 \mu\text{m}$ (0.62 eV) determined from a fit to the ellipsometry data with a parametric semiconductor model.

Sample	x	$1 - x$	t (μm)	r (\AA)	ϵ_∞	A	GaAs-like			GaP-like			E_0 (eV)	n	
							Ω_{TO} (cm^{-1})	Γ_{TO} (cm^{-1})	Ω_{LO} (cm^{-1})	A	Ω_{TO} (cm^{-1})	Γ_{TO} (cm^{-1})			Ω_{LO} (cm^{-1})
GaAs ^a	0	1	NA	93	10.7	1.96(2)	268.2(2)	2.2(2)	291.7	NA	NA	NA	NA	1.42	3.35
205B	0.205	0.795	10.8	36	9.5	1.32(6)	269.9(6)	5.1(8)	288.0	0.80(3)	352.5(7)	23(1)	367.0	1.72	3.24
235B	0.232	0.768	24.3	44	10.2	1.36(3)	270.1(3)	4.6(4)	287.5	0.66(1)	354.9(3)	15(1)	366.2	1.76	3.26
237B	0.24	0.76	22.9	32	10.1	1.30(3)	270.0(3)	4.8(4)	286.9	0.61(1)	355.9(3)	13.2(5)	366.5	1.76	3.26
213B	0.245	0.755	28.8	46	9.8	0.83(2)	271.4(4)	4.6(7)	282.7	1.28(2)	356.2(4)	17.6(6)	378.7	1.76	3.24
213F ^b	0.275	0.725	33.5	80	9.9	1.83(7)	267.3(6)	6.9(1)	291.0	0.91(2)	352.8(4)	19(1)	368.7		noisy
208B	0.435	0.565	12.4	45	9.8	0.82(3)	272.6(5)	4.6(6)	283.8	1.07(2)	356.9(3)	14.6(6)	375.9	1.98	3.19
208F	0.475	0.525	11.7	58	9.7	0.73(3)	272.8(5)	3.9(7)	282.9	1.24(2)	358.5(4)	13.7(6)	380.7	2.03	3.18
225B	0.615	0.385	7.3	48	9.5	0.44(3)	272.1(8)	5(1)	278.3	1.55(2)	357.7(4)	13(1)	385.8	2.26	3.13
226B	0.71	0.29	8.9	41	9.5	0.43(3)	273.2(7)	5(1)	279.3	1.61(2)	360.0(3)	10(1)	389.3	2.29	3.13
209B ^b	0.81	0.19	14	52	8.6	0.19(4)	267(2)	5(f)	269.9	1.83(2)	361.4(4)	9.0(6)	398.0	2.50	3.00
GaP ^a	1	0	NA	45	8.9	NA	NA	NA	NA	1.98(1)	364.8(1)	2.0(1)	403.3	2.70	3.03

^aResults from this work are in good agreement with Refs. 3–6. ^bNo specular reflection from a red laser beam.

cm^{-1} , but was small in other areas. The imaginary part of the pseudodielectric function (ϵ_2) has a deep minimum at 291 cm^{-1} with negative values. This cannot happen for a bulk sample and we attribute this minimum to the Berreman artifact,^{31,32} which occurs at the LO frequency of the GaAs substrate, shown by the vertical dotted line in Fig. 1. The real part (ϵ_1) has a strong discontinuity at this energy.

Apart from this Berreman artifact, the pseudodielectric function can mostly be interpreted similar to the dielectric function of a bulk $\text{GaAs}_{1-x}\text{P}_x$ alloy. (ϵ_2) has maxima at 272 and 354 cm^{-1} , which are taken as the TO energies of the GaAs-like and GaP-like phonons, respectively. (Of course, some smaller features are due to the finite layer thickness.) The real part (ϵ_1) has Kramers-Kronig consistent features expected of two Lorentz oscillators.⁶

The spectrum for sample 225B was fitted with a sum of two Lorentzian oscillators to describe the GaAs-like and GaP-like phonons, shown by dotted lines in Fig. 1. Parameters obtained from the fit are given in Table SI. The corresponding LO energies were estimated from the Lyddane-Sachs-Teller relation (2). Solid (dashed) vertical lines in Fig. 1 show the TO (LO) energies obtained from this fit. There is qualitative agreement, especially for the pseudodielectric function, but the agreement could be better. As expected, two Lorentzians are not sufficient to describe the complex vibrational spectra of the $\text{GaAs}_{1-x}\text{P}_x$ alloy.

We now focus our attention on the ellipsometric angle ψ for sample 225B. This angle rises initially towards a peak located between 272 and 276 cm^{-1} (showing a

small dependence on the angle of incidence). This rising slope is identified with the lower edge of the GaAs-like reststrahlen band. This first peak is followed by a second peak at 288 cm^{-1} associated with the Berreman artifact of the substrate. After a minimum at 325 cm^{-1} due to interference effects, ψ rises again towards a double-peak from 350 to 400 cm^{-1} . This is the GaP-like reststrahlen band. The fit to this GaP-like band with a single Lorentzian (dotted) is particularly poor. As discussed by Humlíček,^{9,30} the impact of a weak absorption feature is amplified, if it occurs within a reststrahlen band. The shape of this GaP-like reststrahlen band allows the conclusion that the main GaP-like TO/LO phonon pair has energies of about 355 and 400 cm^{-1} , with a second weaker absorption peak located within these boundaries. It is difficult to interpret the ellipsometric angle Δ , because it changes very rapidly with photon energy and wraps around by 2π four times within our spectral window. Finally, we discuss the loss function for sample 225B. As shown in Fig. 1, $\text{Im}(-1/\langle\epsilon\rangle)$ has strong peaks near, but not exactly at the LO frequencies.

In summary, the main features of the raw ellipsometry data in Fig. 1 for sample 225B can be interpreted if the GaAs-like and GaP-like reststrahlen bands and the Berreman artifact at the TO energy of the GaAs substrate are taken into account. There are also small modifications due to the finite thickness of the alloy (interference effects).

Since a fit to the data with two Lorentzians to describe the GaAs-like and GaP-like vibrations was only partially successful, we added a second (weaker) GaP-like TO phonon, as suggested by the percolation theory

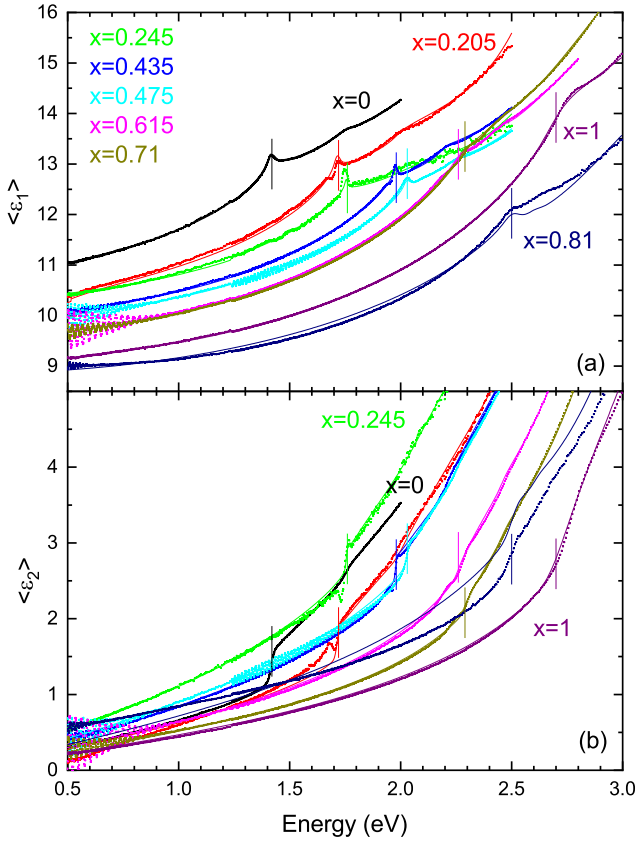


FIG. S2. Real (a) and imaginary part (b) of the pseudodielectric function (ϵ) for selected concentrations of $\text{GaAs}_{1-x}\text{P}_x$ alloy layers on GaAs. Data are shown by symbols. The lines represent the best fit with a parametric semiconductor model as described in the text. The short vertical lines show the location of the direct band gap E_0 obtained from the fit.

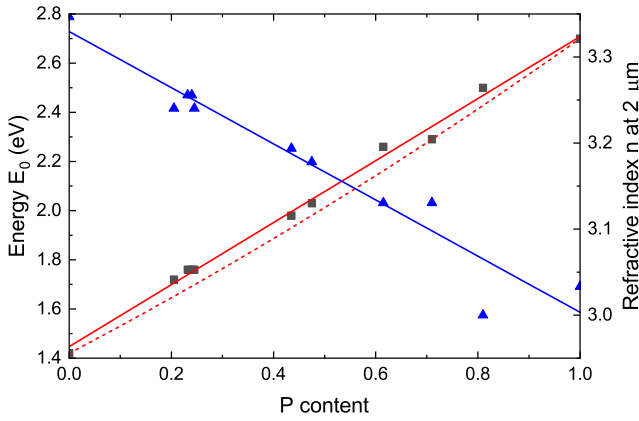


FIG. S3. Direct band gap E_0 (■) and refractive index n at a wavelength of $2 \mu\text{m}$ (▲) of thick $\text{GaAs}_{1-x}\text{P}_x$ alloys on GaAs as a function of P content, determined from ellipsometry. The solid lines show a linear fit, the dashed line includes a bowing parameter of $b = -0.19$ eV for the variation of the direct band gap with composition.

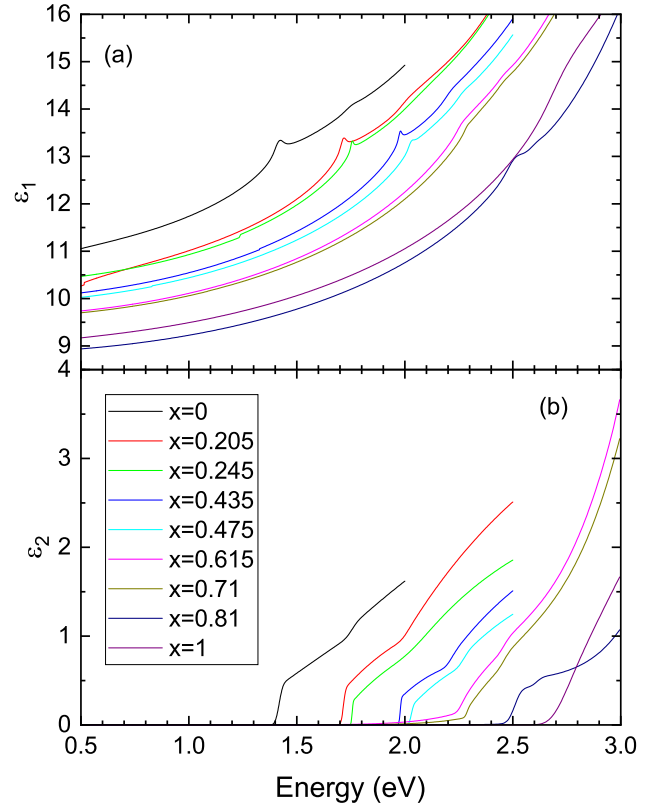


FIG. S4. Real (a) and imaginary part (b) of the dielectric function ϵ for selected concentrations of $\text{GaAs}_{1-x}\text{P}_x$ alloy layers on GaAs, determined from a parametric semiconductor oscillator fit as described in the text.

of Pagès *et al.*¹⁵, at an energy of about 12 cm^{-1} above the stronger one. This reduced the mean standard deviation (weighted by errors), also called MSE, by about 20%, but still did not provide a good description of ψ in the GaP-like reststrahlen region.

The agreement between the model and the data for sample 225B can be improved further if a total of eight Lorentzian oscillators are introduced to describe the lattice absorption. Results are shown by the solid lines in Fig. 1. Even such a large number of oscillators does not achieve a perfect fit to the data. It is questionable whether such a large number of Lorentzian parameters carries physical significance. We believe that our FTIR ellipsometry data do not contain enough information to perform meaningful fits with 6 to 10 Lorentzian for comparison with energies and amplitudes predicted by the cluster model theory, which was carried out in Ref. 14.

S3. ADDITIONAL FIGURE

Figure 3 in the main text showed only the imaginary part of the dielectric function in the reststrahlen region. The corresponding real part is shown in Fig. S1.

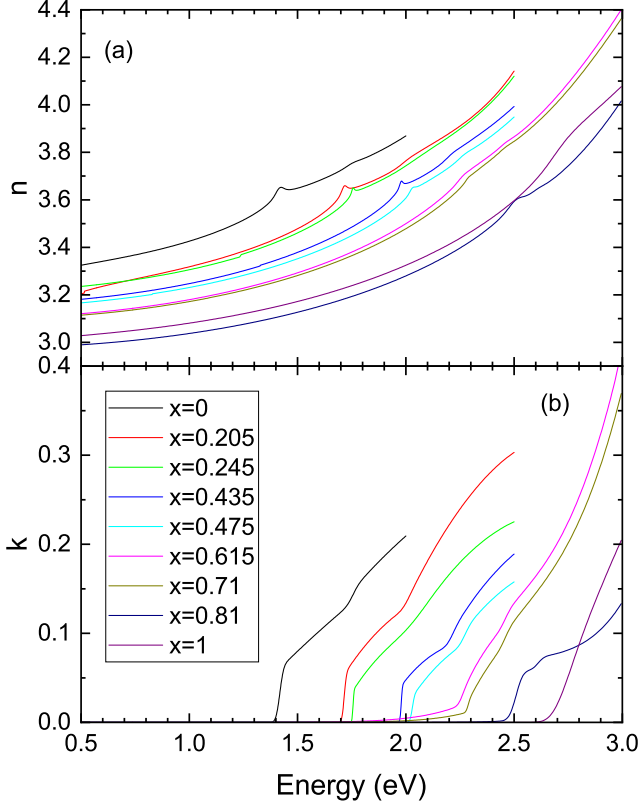


FIG. S5. Same data as in Fig. S4, but displayed as the real (a) and imaginary part (b) of the complex refractive index $n + ik$ for selected concentrations of $\text{GaAs}_{1-x}\text{P}_x$ alloy layers on GaAs, determined from a parametric semiconductor oscillator fit as described in the text.

S4. ELLIPSOMETRY NEAR THE DIRECT BAND GAP

The ellipsometric Mueller matrices from 55° to 80° in 5° increments were also acquired from 210 to 2500 nm on a J.A. Woollam dual rotating compensator ellipsometer (model RC2-XI+) with 60 s integration time per angle. The ellipsometric angles (diagonal blocks of the Mueller matrices) were fitted with two M_0 parametric semiconductor oscillators for the E_0 and $E_0 + \Delta_0$ critical points. For P contents above 60%, an M_1 oscillator for the E_1 critical point was also added. The $E_0 + \Delta_0$ critical point was barely noticeable in the spectra due to broadening. Therefore, Δ_0 was interpolated linearly with composition between the binary end points and treated as a fixed parameter. The fit range was restricted from 0.5 to 2.5 eV for the lower P contents and 0.5 to 3.0 eV for the higher P contents. The surface layer thickness was treated as an additional parameter using the Bruggeman effective medium approximation with a 50% void fraction, with results similar to those given in Table SI. For the thinner samples, weak interference fringes were noticed at the longest wavelengths. Those were ignored in the modeling and the alloy was taken as a bulk substrate.

The resulting pseudodielectric functions near the di-

rect band gap are shown in Fig. S2. In general, the E_0 critical point can clearly be identified as a peak in the $\langle \epsilon_1 \rangle$ spectra for direct alloys ($x < 45\%$). It also leads to a step in $\langle \epsilon_2 \rangle$. For the indirect alloys ($x > 45\%$), the short intervalley scattering times from the Γ -point to the X -valleys broaden the E_0 critical point significantly.^{26,33} That makes it more difficult to locate the direct band gap E_0 for the indirect alloys. We rely more on the data fitting procedure for these alloys to find E_0 . We have marked the location of the E_0 gaps with short vertical lines in Fig. S2. The monotonic increase of E_0 with P content x is quite apparent. For some alloys, especially $x = 0.205$ and $x = 0.435$, the direct band gap E_0 has some fine structure caused by the compositional variations in the layers. The band gap of bulk GaAs was found to be 1.42 eV, as expected. The band gap of bulk GaP (2.70 eV) was about 0.08 eV lower than expected.^{33,34} Most likely, this is due to doping. The LO phonon energy for this bulk GaP substrate was also found to be larger than expected, see Table SI, consistent with a plasma frequency of 60 cm^{-1} and an electron concentration on the order of $1.3 \times 10^{17} \text{ cm}^{-3}$, see Ref. 35. The broadening of the E_0 critical point for this bulk GaP substrate is also larger than expected.³³ (A detailed lineshape analysis using derivatives is not possible with RC2 ellipsometry data.)

The pseudo-refractive index at long wavelengths (the square root of $\langle \epsilon_1 \rangle$) also increases monotonically with P content, with the exception for the alloy with 81% P. The composition of this alloy seems correct, as given by the location of the direct band gap E_0 . However, its refractive index is lower than it should be. Most likely, this alloy has embedded voids, which reduce the refractive index following the Bruggeman effective medium theory.

The location of the direct band gap can also be identified by steps in the $\langle \epsilon_2 \rangle$ spectra, especially for the direct alloys with $x < 0.45$. On the other hand, the magnitude of the $\langle \epsilon_2 \rangle$ spectra at low energies depends mostly on the surface roughness and therefore varies greatly between samples with no apparent trends.

The direct band gap E_0 and the refractive index n at $2 \mu\text{m}$ wavelength are listed in Table SI and also plotted in Fig. S3 as a function of composition. The rise of E_0 is nearly linear with increasing P content, as shown by the solid line. Our errors are too large to determine the bowing parameter. The expected dependence²⁶ of E_0 versus P content with a bowing parameter of $b = -0.19 \text{ eV}$ is shown by the dotted line, which is not unreasonable in comparison with our results. The decrease of n at $2 \mu\text{m}$ wavelength is also nearly linear, as shown by the solid line. The only exception is the sample with 81% P. It has already been discussed that the low refractive index for this sample is probably due to voids, which result in a relatively lower electron density.

For completeness, we also show the complex dielectric function ϵ and the complex refractive index $n + ik$ obtained from the parametric semiconductor models in Figs. S4 and S5, respectively. No attempts were made to

clean the surfaces, reduce overlayers, or improve the accuracy of the data. Since the agreement with the model and the fit is not always perfect, the data shown in these figures needs to be taken with a grain of salt. They are qualitatively correct, but small deviations should be expected due to the built-in numerical "features" of the parametric semiconductor model. The data confirm the much lower broadenings for the direct alloys with P contents below 45% than for the indirect alloys. We also see systematic variations of the refractive index and the

direct band gap with increasing P content, except for the 81% sample as mentioned above. The alloys with 61.5% and 71% P seem to show absorption below the band gap, but ellipsometry is not really sensitive to low-level indirect absorption processes. While certainly plausible, this might be a numerical artifact. The $E_0 + \Delta_0$ transition is more pronounced in ϵ_2 than in the raw experimental data expressed as a pseudodielectric function $\langle \epsilon_2 \rangle$, but this might also be a numerical artifact due to the built-in bias of the parametric semiconductor model.